# Efficient computational method for joint distributions of heights and periods of nonlinear ocean waves

Yingguang Wang [a, b, c, *]

[a] State Key Laboratory of Ocean Engineering, Shanghai Jiao Tong University, Shanghai, 200240, China
[b] Collaborative Innovation Center for Advanced Ship and Deep-Sea Exploration(CISSE), Shanghai, 200240, China
[c] School of Naval Architecture, Ocean and Civil Engineering, Shanghai Jiao Tong University, Shanghai, 200240, China

## ARTICLE INFO

## ABSTRACT

This paper proposes a novel method for efficient prediction of joint distributions of heights and periods of nonlinear ocean waves. The proposed novel method utilizes a transformed linear simulation which is based on a Hermite transformation model where the transformation is chosen to be a monotonic cubic polynomial, calibrated such that the first four moments of the transformed model match the moments of the true process. This proposed novel method is utilized to predict the joint distributions of wave heights and periods of a sea state with the surface elevation data measured at the Gulfaks C platform in the North Sea, and the novel method's accuracy and efficiency are favorably validated by using comparisons with the results from an empirical joint distribution model, from a linear simulation model and from a second-order nonlinear simulation model.

## 1. Introduction

Accurate prediction of joint distributions of wave heights and periods is of vital importance to the design and safety analysis of ships and floating offshore structures. Firstly, wave breaking (a phenomenon that can lead to the risk of ship capsizing) takes place when wave height and period cannot maintain the equilibrium condition needed for stability. Therefore, it is necessary to have the knowledge of the joint distribution of the wave heights and the associated wave periods in order to predict the possibility of the occurrence of wave breaking (see e.g. Liu et al., 2015, 2016; Perlin et al., 2013) in a given sea state. Secondly, in the design of a floating offshore structure it is very important to take into consideration of the joint probability distribution of wave height and period. This is because one of the most important considerations for the design of a floating offshore structure is to avoid the occurrence of resonant motion which occurs when wave periods are close to the natural motion period of the floating offshore structure. If the wave period is sufficiently long or sufficiently short in comparison with the natural period of the floating offshore

structure's motion, the offshore structure may be in no danger even if the wave height is relatively large. On the contrary, the motion response will reach a level critical for the floating offshore structure if wave periods are close to the structure's natural period (see Ochi, 2005). In designing a floating offshore structure, it is therefore very important to know the statistical information about the wave heights having periods that are close to the structure's natural period in the areas where the floating offshore structure will be installed and operated.

Waves in the real world are random in nature. In the literature, there exist some empirical (or theoretical) models of joint distributions of wave heights and periods of random ocean waves (see e.g. Cavanié et al., 1976; Lindgren and Rychlik, 1982; Longuet-Higgins, 1975; Longuet-Higgins, 1983; Stansell et al., 2004). However, the previous research work of Wang and Xia (2012) has shown that such kind of empirical (or theoretical) formulas will sometimes predict wave characteristic distributions that differ considerably from the true ones. In order to overcome the weakness of the empirical (or theoretical) approach for predicting the joint distributions of wave heights and periods, Monte Carlo Simulation (MCS) can be performed through the superposition of harmonics based on a wave spectrum, and in the ocean engineering literature this is also called a linear simulation method. Based on some idealized target spectra, Rodríguez and Soares (1999) and Rodríguez et al. (1999) performed linear simulations to obtain long wave time series and

* Corresponding author.
E-mail address: wyg110@sjtu.edu.cn.

aggregated all the simulated waves into a joint histogram to obtain the joint distributions of wave height and period. However, their simulated waves (and the subsequently obtained joint distributions of wave height and period) are good approximations to the real ones only under the condition of small oscillation amplitudes. Meanwhile, Rodríguez and Soares (1999) and Rodríguez et al. (1999) did not verify their research results with field data.

Starting from a specific wave power spectral density function, there is another approach to obtain the joint distributions of wave height and period by using a nonlinear simulation method. Wang and Xia (2012) used a nonlinear simulation method to compute the wave surface elevations for nonlinear random ocean waves. In their numerical implementation, they divided the problem into two processes, i.e. first generating a first order linear (Gaussian) wave process with a specific wave spectrum, then correcting it by adding the simulated second order nonlinear wave process. Their obtained time histories of waves were then statistically processed to obtain the joint distribution of wave height and period. However, in their simulation project there were a huge number of second order corrections that need to be evaluated. Therefore, using the nonlinear simulation method for predicting the joint distributions of wave height and period has become very time consuming, laborious and unsuitable for practical implementations.

In order to improve the simulation efficiency, a novel approach for predicting the joint distributions of wave heights and periods by utilizing a transformed linear simulation method will be first proposed in this article. The proposed transformed linear simulation method will be based on a Hermite transformation model where the transformation is chosen to be a monotonic cubic polynomial, calibrated such that the first four moments of the transformed model match the moments of the true process. The proposed new approach will be utilized to predict the joint distributions of wave heights and periods of a sea state with the surface elevation data measured at the Gulfaks C platform in the North Sea, and its accuracy and efficiency will be validated by using comparisons with the results from an empirical joint distribution model, from a linear simulation model and from a second-order nonlinear simulation model.

## 2. The nonlinear random sea waves and the proposed transformed linear simulation method

Waves in an idealized linear Gaussian random sea have crest-trough symmetry. However, it is known that waves in the real sea are nonlinear, and the ocean surface elevation process deviates from the Gaussian assumption, i.e. the wave crests are becoming steeper and higher and the wave troughs are becoming flatter and shallower than expected under the Gaussian assumption. In the following we briefly introduce the theories of the nonlinear random sea waves.

For an idealized flow, the flow velocity can be described as the gradient of a velocity potential $\Phi(x,y,z,t)$ in which $x$ and $y$ are the horizontal Cartesian coordinates, $z$ is the vertical Cartesian coordinate and $t$ is time. The positive $z$-direction points upward. The free surface is located at $z = \eta(x, y, t)$, and the bottom of the fluid region is at $z = -d(x,y)$. Assuming incompressible flow, the velocity field is divergence-free and the velocity potential $\Phi(x,y,z,t)$ satisfies Laplace's equation

$$\nabla^2 \Phi = 0 \tag{1}$$

The free-surface boundary conditions for surface gravity waves − using a potential flow description − consist of a kinematic and a dynamic boundary condition. The kinematic boundary condition ensures that the normal component of the fluid's flow velocity $(\partial\Phi/\partial x,\ \partial\Phi/\partial y,\ \partial\Phi/\partial z)^T$ at the free surface equals the normal velocity component of the free-surface motion $z = \eta (x, y, t)$:

$$\frac{\partial\eta}{\partial t} + \frac{\partial\Phi}{\partial x}\frac{\partial\eta}{\partial x} + \frac{\partial\Phi}{\partial y}\frac{\partial\eta}{\partial y} = \frac{\partial\Phi}{\partial z}\ at\ z = \eta(x,y,t) \tag{2}$$

The dynamic boundary condition states that, without surface tension effects, the atmospheric pressure just above the free surface equals the fluid pressure just below the surface. For an unsteady potential flow this means that the Bernoulli equation is to be applied at the free surface. In case of a constant atmospheric pressure, the dynamic boundary condition becomes:

$$\frac{\partial\Phi}{\partial t} + \frac{1}{2}\left[\left(\frac{\partial\Phi}{\partial x}\right)^2 + \left(\frac{\partial\Phi}{\partial y}\right)^2 + \left(\frac{\partial\Phi}{\partial z}\right)^2\right] + g\eta = 0\ at\ z = \eta(x,y,t) \tag{3}$$

where the constant atmospheric pressure has been taken equal to zero, without loss of generality. For permanent waves above a horizontal bed, the mean depth $d$ is a constant and the boundary condition at the bed becomes:

$$\frac{\partial\Phi}{\partial z} = 0\ \ at\ z = -d \tag{4}$$

Using a perturbation-series approach (Stokes expansion), solutions of the system (1)–(4) can be sought using the following equations (see, e.g. Toffoli et al. (2006)):

$$\begin{cases} \Phi = \Phi^{(1)} + \Phi^{(2)} + \cdots \\ \eta = \eta^{(1)} + \eta^{(2)} + \cdots \end{cases} where \frac{\Phi^{(n+1)}}{\Phi^{(n)}} = \frac{\eta^{(n+1)}}{\eta^{(n)}} = O(\tilde{\varepsilon}) \tag{5}$$

In Eq. (5) $\tilde{\varepsilon}$ is a small parameter in the expansion and it is typically proportional to the wave steepness. For a random sea state characterized by a specific wave power spectral density function $S_\eta(\omega)$ where $\omega$ is the radian frequency, it can be shown that a first order linear Gaussian solution of the system (1)–(5) has the following form ((see, e.g. Toffoli et al. (2006); Ma et al. (2010))):

$$\Phi^{(1)}(x,t) = Re\sum_{n=0}^{N}\frac{igc_n}{\omega_n}\frac{\cosh k(z+d)}{\cosh kd}\exp(i(\omega_n t - k_n x + \varepsilon_n)) \tag{6}$$

$$\eta^{(1)}(x,t) = Re\sum_{n=0}^{N} c_n \exp(i(\omega_n t - k_n x + \varepsilon_n)) \tag{7}$$

as $N$ tends to infinity. In Eqs. (6) and (7), Re denotes the real part of the complex number, and for each elementary cosine wave $c_n$ denotes its complex valued amplitude which is directly related to the specific wave power spectral density function $S_\eta(\omega)$ by the relation $E[|c_n|^2] = S_\eta(\omega_n)\Delta\omega$. In Eqs. (6) and (7), $\omega_n$ is the radian frequency and $\omega_n = n\Delta\omega = n(\omega_c/N)$, and $\omega_c$ is the upper cut off frequency beyond which the wave spectrum $S_\eta(\omega)$ may be assumed to be zero for either mathematical or physical reasons. $k_n$ is the wave number, and $\varepsilon_n$ is the phase angle uniformly distributed in the interval [0, $2\pi$]. Furthermore, the individual frequencies $\omega_n$ and wave numbers $k_n$ in Eqs. (6) and (7) are functionally related through the following equation:

$$\omega_n^2 = gk_n \tanh(k_n d) \tag{8}$$

where $g$ is the gravitational acceleration and $d$ is the water depth. The traditional **linear simulation method** in the ocean engineering practice is to numerically implement Eqs. (7) and (8) to

generate the first order, linear (Gaussian) wave time histories at a specific location of the sea. However, waves in the real sea are nonlinear and non-Gaussian. Therefore, the linear Gaussian sea model as expressed in Eqs. (7) and (8) should be corrected by including second-order (quadratic) terms. Following Langley, (1987) and Hasselmann, (1962) the second-order (quadratic) corrections are given by:

$$
\Phi^{(2)}(x,t) = 2\text{Re} \sum_{n=0}^{N} \sum_{m=-0}^{N} ic_n c_m P(\omega_n, \omega_m) \frac{\cosh(k_n + k_m)(z + d)}{\cosh(k_n + k_m)d} \exp(i(\omega_n t - k_n x + \varepsilon_n))
$$
$$
\exp(i(\omega_m t - k_m x + \varepsilon_n)) + 2\sum_{n=0}^{N} \frac{c_n^2 g k_n}{\sinh 2k_n h} t
$$
(9)

$$
\eta^{(2)}(x,t) = \text{Re} \sum_{m=0}^{N} \sum_{n=0}^{N} c_m c_n [r_{mn} \exp(i(\omega_m t - k_m x + \varepsilon_m + \omega_n t - k_n x + \varepsilon_n))
$$
$$
+ q_{mn} \exp(i(\omega_m t - k_m x + \varepsilon_m - \omega_n t + k_n x - \varepsilon_n))]
$$
(10)

In the above two equations $P(\omega_n, \omega_m)$, $r_{mn}$ and $q_{mn}$ are called second-order (quadratic) transfer functions. The quadratic transfer function $P(\omega_n, \omega_m)$ is given by:

$$
P(\omega_n, \omega_m) = (1 - \delta_{-n,m}) \frac{\frac{g^2 k_n k_m}{2\omega_n \omega_m} - \frac{1}{4}(\omega_n^2 + \omega_m^2 + \omega_n \omega_m) + \frac{g^2}{4} \frac{(\omega_n k_m^2 + \omega_m k_n^2)}{\omega_n \omega_m (\omega_n + \omega_m)}}{(\omega_n + \omega_m) - g \frac{k_n + k_m}{(\omega_n + \omega_m)} \tanh((k_n + k_m)d)}
$$
(11)

In the above equation $\delta_{-n,m}$ is the Kroenecker delta whose value equals unity if n + m = 0. $\delta_{-n,m} = 0$ if n + m ≠ 0. This Kroenecker delta ($\delta_{-n,m}$) is introduced to avoid a singular $P(\omega_n, \omega_m)$.

The quadratic transfer functions $r_{mn}$ and $q_{mn}$ are given by:

In the above two equations the wave numbers $k_n$ and frequencies $\omega_n$ satisfy the same relation as in the linear case. Finally, by combining Eqs. (7) and (10) the wave surface elevations for the nonlinear random ocean waves can be written as:

$$
\eta(x,t) = \eta^{(1)}(x,t) + \eta^{(2)}(x,t) = \text{Re} \sum_{n=0}^{N} c_n \exp(i(\omega_n t - k_n x + \varepsilon_n)) +
$$
$$
\text{Re} \sum_{m=0}^{N} \sum_{n=0}^{N} c_m c_n [r_{mn} \exp(i(\omega_m t - k_m x + \varepsilon_m + \omega_n t - k_n x + \varepsilon_n))
$$
$$
+ q_{mn} \exp(i(\omega_m t - k_m x + \varepsilon_m - \omega_n t + k_n x - \varepsilon_n))]
$$
(14)

The traditional **nonlinear simulation method** in the ocean engineering practice is to numerically implement Eqs. (14) and (8) to generate the nonlinear wave time histories at a specific location

$$
r_{mn} = -\left(\frac{1}{g}\right) \left( \frac{\left(\frac{1}{4\omega_m \omega_n}\right) 2(\omega_m + \omega_n)\left(\omega_n^2 \omega_m^2 - k_n k_m g^2\right) + \omega_n\left(\omega_m^4 - g^2 k_m^2\right) + \omega_m\left(\omega_n^4 - g^2 k_n^2\right)}{(\omega_m + \omega_n)^2 \cosh((k_m + k_n)d) - g(k_m + k_n)\sinh((k_m + k_n)d)} \right)
$$
$$
(\omega_m + \omega_n)\cosh((k_m + k_n)d) - \left(\frac{1}{4g\omega_m \omega_n}\right)\left(k_m k_n g^2 - \omega_n^2 \omega_m^2\right) + \left(\frac{1}{4g}\right)\left(\omega_m^2 + \omega_n^2\right)
$$
(12)

$$
q_{mn} = -\left(\frac{1}{g}\right) \left( \frac{\left(\frac{1}{4\omega_m \omega_n}\right) 2(\omega_m - \omega_n)\left(\omega_n^2 \omega_m^2 + k_n k_m g^2\right) - \omega_n\left(\omega_m^4 - g^2 k_m^2\right) + \omega_m\left(\omega_n^4 - g^2 k_n^2\right)}{(\omega_n - \omega_m)^2 \cosh(|k_m - k_n|d) - g|k_n - k_m|\sinh(|k_n - k_m|d)} \right)
$$
$$
(\omega_n - \omega_m)\cosh(|k_n - k_m|d) - \left(\frac{1}{4g\omega_m \omega_n}\right)\left(k_m k_n g^2 + \omega_n^2 \omega_m^2\right) + \left(\frac{1}{4g}\right)\left(\omega_m^2 + \omega_n^2\right)
$$
(13)

of the sea. For the numerical implementation of the nonlinear simulation, the problem is usually divided into two processes, i.e. first generating the first order, linear (Gaussian) time histories with a specific wave spectrum at a specific location, for each of these the numerical algorithm then evaluates the full set of second order corrections according to the hydrodynamic theory as specified in this Section. Therefore, the first order wave process, with $N$ components at frequencies $\omega_n$, gives rise to a total of $N^2$ corrections, spreading over all sum frequencies at frequencies $\omega_n + \omega_m$, and to another $N^2$ corrections over all difference frequencies $\omega_n - \omega_m$. However, the nonlinear simulation method as explained above will become very time consuming when $N$ becomes large. In order to overcome this drawback, we propose to utilize a transformed linear simulation method in this paper for predicting the wave heights and periods joint distributions, and in the following the theoretical background of this method will be elucidated.

Our proposed transformed linear simulation method is an alternative and faster method than including the second order correction terms to the linear model. It will use a deterministic and time instantaneous functional transformation. The non-Gaussian wave elevation process, $\eta(x, t)$ is then a function of a single Gaussian process, $\eta^{(1)}(x, t)$:

$$\eta(x, t) = G\left(\eta^{(1)}(x, t)\right) \tag{15}$$

where $G(\cdot)$ is a continuously differentiable function with positive derivative. In this article, the $G(\cdot)$ function is proposed to be based on a Hermite transformation model. This transformation is chosen to be a monotonic cubic polynomial, which is calibrated such that the first four moments of the transformed model match the moments of the true process. In the following we write $\eta^{(1)}(x, t)$ as $\hat{z} = \eta^{(1)}(x, t)$. First we give the definition of Hermite polynomials. The Hermite polynomials of degree $n$, denoted by $H_n(\hat{z})$, is defined as a function which satisfies the relationship given by

$$\frac{d^n}{d\hat{z}^n}\exp\left(-\frac{\hat{z}^2}{2}\right) = (-1)^n H_n(\hat{z})\exp\left(-\frac{\hat{z}^2}{2}\right) \tag{16}$$

We next define the notion of a "Hermite moment" $h_n$ as (see e.g. Wang, (2014)):

$$h_n = \frac{1}{n!}E[H_n(\hat{z})] \tag{17}$$

We can then use the following formula for calculating the $G(\cdot)$ function (see e.g. Wang, (2014)):

$$G(\hat{z}) = \hat{m}_\eta + \hat{k}\sigma_\eta\left[\hat{z} + \tilde{h}_3\left(\hat{z}^2 - 1\right) + \tilde{h}_4\left(\hat{z}^3 - 3\hat{z}\right) + ...\right] \tag{18}$$

In the above equation $\hat{m}_\eta$ and $\sigma_\eta$ are respectively the mean and standard deviation of the surface elevation process $\eta(x, t)$. The coefficient $\hat{k}$ is a scaling factor, while the coefficients $\tilde{h}_n$ may be related to the Hermite moments $h_n$ in Eq. (17) by applying a Hermite polynomial to Eq. (18) and take expectations. For $N = 4$ moments, the solution is (see e.g. Wang, (2014)):

$$\tilde{h}_3 = \frac{\rho_3}{6}(1 - 0.015|\rho_3| + 0.3\rho_3 2)/(1 + 0.2(\rho_4 - 3)) \tag{19}$$

$$\tilde{h}_4 = 0.1 \times \left((1 + 1.25(\rho_4 - 3))^{1/3} - 1\right)$$
$$\times \left(1 - 1.43\rho_3^2/(\rho_4 - 3)\right)^{(1 - 0.1\rho_4^{0.8})} \tag{20}$$

In the above two equations the $\rho_3$ and $\rho_4$ are respectively the skewness and kurtosis of the surface elevation process $\eta(x, t)$. The

above Eqs. (18)-(20) are the core procedures within the "transformed linear simulation method" proposed in this article. Meanwhile, we can obviously see that the accuracy of the functional transformation calculated according to Eq. (18) depends on how many moments are kept during the calculation. The more moments are kept, the more accurate the functional transformation will be. From the above mentioned derivation process it can be noted that in order to calculate the $G(\cdot)$ function, we need to know the values of the mean, standard deviation, skewness and kurtosis of the second order nonlinear random waves. In the following, the detailed mathematical procedures for obtaining these statistical parameters will be illustrated.

Without loss of generality we set the position coordinate $x$ in $\eta(x, t)$ to be $x = 0$. Meanwhile, we also write $\eta(0, t)$ in a simplified way as to be $\eta(t)$. Then, after a lengthy derivation process as shown in Langley (1987), Eq. (14) can be re-written in the following matrix notation:

$$\eta(t) = \mathbf{s}^T\mathbf{X} + \mathbf{X}^T[Q + R]\mathbf{X} + \mathbf{Y}^T[Q - R]\mathbf{Y} \tag{21}$$

where $Q$ and $R$ are real symmetric matrix whose $nm$th components are $s_n s_m q_{mn}$ and $s_n s_m r_{mn}$ respectively, $\mathbf{s}$ is a vector whose $n$th components are $s_n$ ($s_n = \sqrt{S_\eta(\omega_n)d\omega}$). $\mathbf{X}$ and $\mathbf{Y}$ are vectors whose $n$th components are $x_n$ and $y_n$ respectively, and $x_n$ and $y_n$ are Gaussian random variables whose expressions are shown in Langley (1987). By performing an eigenvalue decomposition, the above equation becomes:

$$\eta(t) = \mathbf{s}^T\mathbf{X} + \mathbf{X}^T P_1^T \Lambda_1 P\mathbf{X} + \mathbf{Y}^T P_2^T \Lambda_2 P_2\mathbf{Y} \tag{22}$$

where $\Lambda_1$ is a diagonal matrix with the eigenvalues of the matrix $[Q + R]$ in the respective diagonal and $P_1$ contains the corresponding eigenvectors per row. Meanwhile, $\Lambda_2$ is a diagonal matrix with the eigenvalues of the matrix $[Q - R]$ in the respective diagonal and $P_2$ contains the corresponding eigenvectors per row. Introducing a new set of Gaussian random variables $Z_j$, such that:

$$\mathbf{Z} = \begin{bmatrix} \mathbf{P}_1 & 0 \\ 0 & \mathbf{P}_2 \end{bmatrix}\begin{bmatrix} \mathbf{X} \\ \mathbf{Y} \end{bmatrix} \tag{23}$$

We can then write the stochastic process $\eta(t)$ as (this is called the Kac-Siegert solution):

$$\eta(t) = \sum_{j=1}^{2N} \beta_j Z_j + \lambda_j Z_j^2 \tag{24}$$

where $Z_j$ are independent Gaussian processes with unit variance, and $\beta_j$ and $\lambda_j$ are coefficients computed based on the information provided by the wave power spectral density function $S_\eta(\omega)$, which is chosen for a given sea state. Specifically, the coefficients in the above equation are computed as follows:

$$\boldsymbol{\beta} = \begin{bmatrix} \mathbf{P}_1\mathbf{s} \\ 0 \end{bmatrix} \tag{25}$$

$$\boldsymbol{\lambda} = \begin{bmatrix} (\Lambda_1)^d \\ (\Lambda_2)^d \end{bmatrix} \tag{26}$$

where $(\Lambda_i)^d$ denotes a column vector formed by the diagonal elements of $\Lambda_i$. Having obtained the values of $\beta_j$ and $\lambda_j$, the values of the mean, standard deviation, skewness and kurtosis of the second order nonlinear random waves can then be calculated as (Langley (1987)):
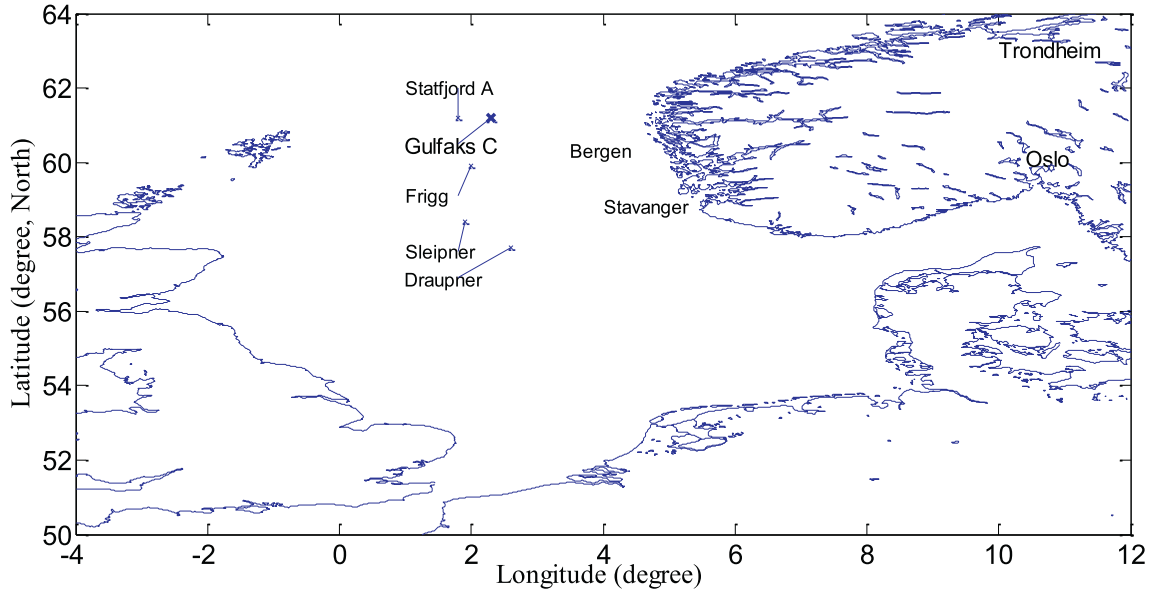
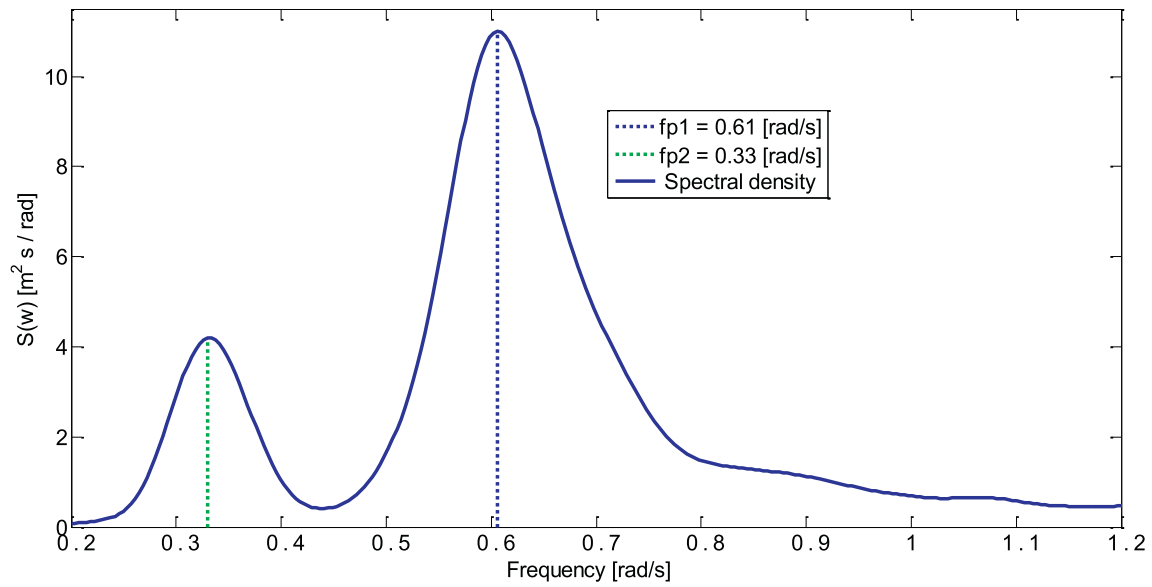**Fig. 1.** The geographical position of the Gulfaks C platform in the North Sea.



**Fig. 2.** The wave spectrum corresponding to the measured surface elevation data at the Gulfaks C platform.

$$\widehat{m}_\eta = \sum_{j=1}^{2N} \lambda_j \tag{27}$$

$$\sigma_\eta = \sqrt{\sum_{j=1}^{2N} \beta_j^2 + 2\sum_{j=1}^{2N} \lambda_j^2} \tag{28}$$

$$\rho_3 = \frac{\left[ 6\sum_{j=1}^{2N} \lambda_j \beta_j^2 + 8\sum_{j=1}^{2N} \lambda_j^3 \right]}{\sigma_\eta^3} \tag{29}$$

$$\rho_4 = \frac{3 + 48\sum_{j=1}^{2N} \lambda_j^2 \beta_j^2 + 48\sum_{j=1}^{2N} \lambda_j^4}{\sigma_\eta^4} \tag{30}$$

## 3. A calculation example and discussions

In this Section we will utilize our proposed transformed linear simulation method for calculating the joint distributions of wave height and period of a sea state with the surface elevation data measured at the Gulfaks C platform in the North Sea from 17.00 p.m. to 21.20 p. m. on December 24, 1989. Fig. 1 shows the geographical position of the Gulfaks C platform. This measured data set contains 39,000 measurements, and the sampling rate is 2.5 Hz.
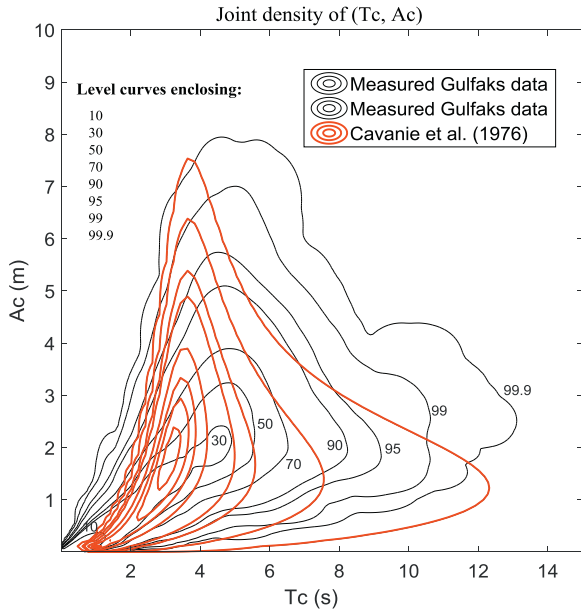
**Fig. 3.** The wave crest height and period joint distributions calculated with different methods (Measured data and Cavanie et al. [5]).
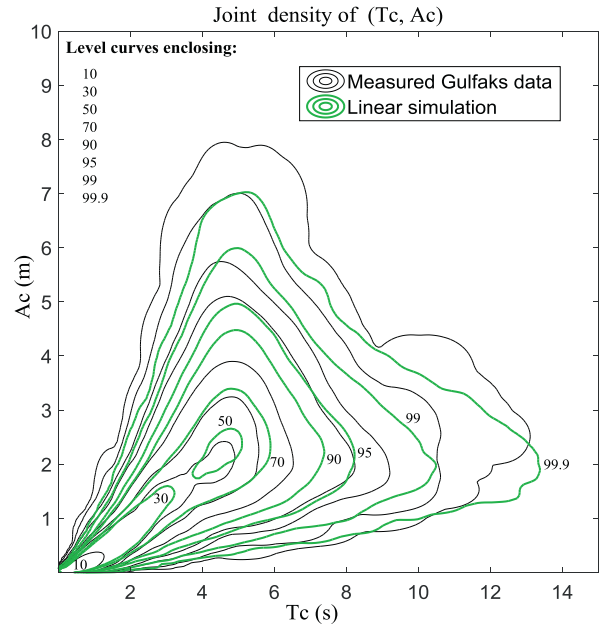


**Fig. 5.** The wave crest height and period joint distributions calculated with different methods (Measured data and linear simulation).
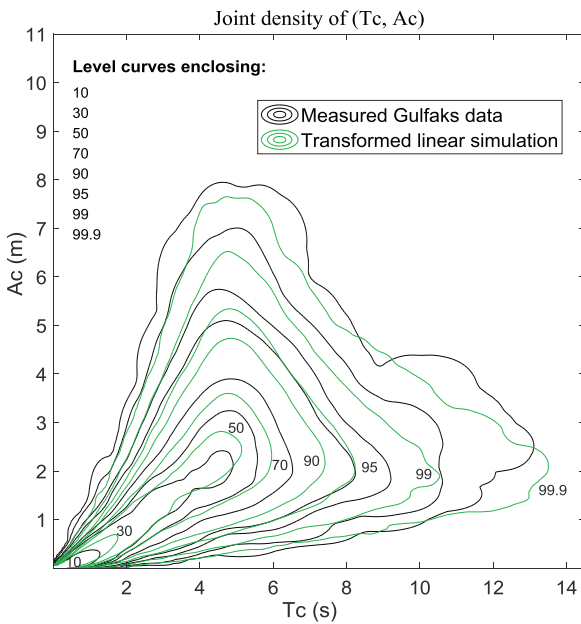


**Fig. 4.** The wave crest height and period joint distributions calculated with different methods (Measured data and Transformed linear simulation).
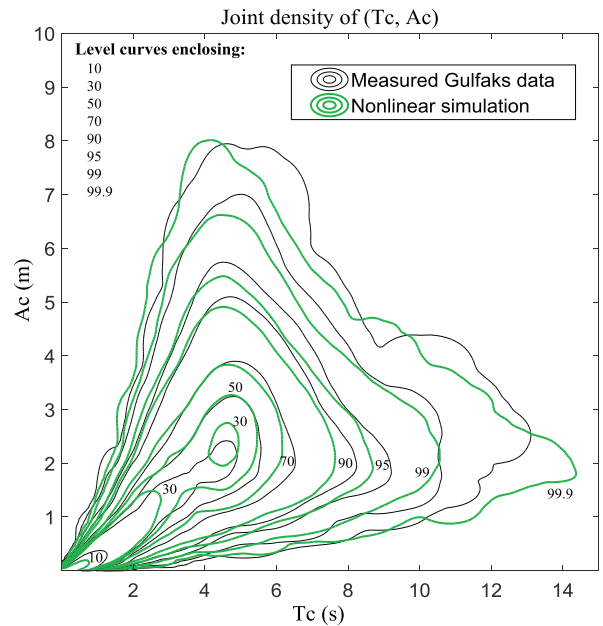


**Fig. 6.** The wave crest height and period joint distributions calculated with different methods (Measured data and nonlinear simulation).

The water depth is 218 m. There are two EMI laser sensors named 219 and 220. This data set is obtained from sensor 219, which is located in the Northwest corner approximately two platform leg diameters away from the closest leg. Thus the wave elevation is not expected to be significantly affected by diffraction effects for incoming waves in the western sector. The significant wave height is Hs = 6.8 m, and the spectral peak period is Tp = 10.5 s. The wind direction for this period is from the south. The wave spectrum for this data set can then be calculated, and is shown in Fig. 2 (Note that the extreme upper tails of the spectrum are not plotted here). Clearly, the wave spectrum is a bimodal one indicating the sea state is a combination of wind waves and swell.

Figs. 3–6 show our calculated joint distributions of wave crest height and period for this measured specific sea state. The solid black lines in Fig. 3 represent the results of the joint distribution of wave crest height and period directly obtained from the measured wave elevation points at the Gulfaks C platform. For obtaining these results, the time series of wave crest height are first extracted from these measured wave elevation points. The time series of wave crest front period and crest back period are also extracted from these measured wave elevation points, and adding these two together we can obtain the time series of wave period. Please note that in this paper the definition of the wave crest front period is the

time span from an up-crossing to the next wave crest, and the definition of the crest back period is the time from a wave crest to the next down-crossing. The wave crest period is a sum value of the wave crest front period and the crest back period. Next, exact Epanechnikov kernel density estimates are carried out for obtaining the joint distribution of wave crest height and period as shown by the black lines in Fig. 3. Here we should mention that some kinds of kernel density functions are commonly used: uniform, biweight, triweight, triangle, tricube, Epanechnikov, Gaussian, and cosine. However, the kernel density function that minimizes the mean integrated square error is the Epanechnikov kernel, which has the following expression:

$$K(h) = \frac{3}{4}\left(1 - h^2\right)\mathbf{1}_{\{|h|\leq 1\}} \tag{31}$$

where $\mathbf{1}_{\{|h|\leq 1\}}$ is the indicator function. We can obviously notice that the joint distribution of wave crest height and period directly obtained from the measured wave elevation data is not symmetrical with respect to the normalized wave period.

The solid red lines in Fig. 3 represent the empirical joint distribution of wave crest height and period as developed in Cavanié et al. [5] that has the following mathematical expressions:

$$f(T_C, A_C) = c\frac{A_C^2}{T_C^5}Exp\left\{ -\frac{A_C^2}{8\varepsilon^2 T_C^4}\left[\left(T_C^2 - \left(\frac{1-\varepsilon^2}{1+\gamma^2}\right)\right)^2 \right.\right.$$
$$\left.\left. + \beta^2\left(\frac{1-\varepsilon^2}{1+\gamma^2}\right)\right]\right\} \tag{32}$$

where

$$c = \frac{1}{4}\left(1 - \varepsilon^2\right)\left(\frac{1}{2\pi}\right)^{0.5}\frac{1}{\varepsilon}\frac{1}{\alpha_2}\left(\frac{1}{1+\gamma^2}\right)^2 \tag{33}$$

$$\alpha_2 = \frac{1}{2}\left(1 + \left(1 - \varepsilon^2\right)^{0.5}\right) \tag{34}$$

$$\beta = \varepsilon^2 / \left(1 - \varepsilon^2\right) \tag{35}$$

$$\varepsilon = \sqrt{1 - \frac{m_2^2}{m_0 m_4}} \tag{36}$$

$$\gamma = \frac{m_0 m_2}{m_1^2} - 1 \tag{37}$$

where $m_0$, $m_1$, $m_2$ and $m_4$ are various orders of spectral moments calculated from the specific wave spectrum as shown in Fig. 2. Obviously in this case the Cavanié et al. [5] joint distribution of wave crest height and period deviates a lot from the corresponding **real** joint distribution obtained directly from the measured data.

In Fig. 4 the solid black lines again represent the results of the joint distribution of wave crest height and period directly obtained from the measured wave elevation points at the Gulfaks C platform. In Fig. 4 the solid green lines represent the results of the joint distribution of wave crest height and period obtained from utilizing our proposed transformed linear simulation method. In applying the transformed linear simulation method, two matrices $[Q + R]$ and $[Q - R]$ as specified in Eq. (21) are first calculated and the elements in these two matrices are directly related to the wave spectrum as shown in Fig. 2 and the quadratic transfer functions $r_{mn}$ and $q_{mn}$. Subsequently the coefficients $\beta_j$ and $\lambda_j$ are calculated

by using Eq. (25) and Eq. (26) based on the wave spectrum as shown in Fig. 2. Having obtained the values of $\beta_j$ and $\lambda_j$, the values of the mean, standard deviation, skewness and kurtosis of the nonlinear random waves can then be calculated by using Eqs. (27)–(30). Finally, the $G(\bullet)$ function is calculated by using Eqs. (18)–(20) in Section 2, and this $G(\bullet)$ function is subsequently used to transform a linearly simulated 2000000 wave elevation points time history from the wave spectrum in Fig. 2 into a non-Gaussian time history. For this non-Gaussian time history the wave crests have become higher and sharper, and the wave troughs have become shallower and flatter (i.e. the waves have become more nonlinear). Next, from this non-Gaussian time history the wave crest height time series are extracted. The wave crest front period and crest back period time series are also extracted from this non-Gaussian time history, and adding these two together we can obtain the wave period time series. Then exact Epanechnikov kernel density estimates are carried out for obtaining the wave crest height and period joint distribution as shown by the green lines in Fig. 4. We can see that the results from the Transformed linear simulation method fit the measured data much better than the results obtained from using the Cavanié et al. [5] joint distribution model. Moreover, we can obviously notice that the joint distribution of wave crest height and period obtained using the Transformed linear simulation method is not symmetrical with respect to the normalized wave period. Finally, it is mentioned that in this case it takes only about 18 s on a desktop computer (HP dx2310MT (VP784PA), Pentium (R) Dual-Core CPU E5300 @2.60GHz) to obtain the green curves in Fig. 4 by utilizing our proposed transformed linear simulation method.

In Fig. 5 the solid black lines again represent the results of the joint distribution of the wave crest height and period directly obtained from the measured wave elevation points at the Gulfaks C platform. In Fig. 5 the solid green lines represent the results of the joint distribution of the wave crest height and period obtained from using the linear simulation method, i.e. by numerically implementing Eqs. (7) and (8) to generate a time series of sea waves with 2000000 elevation points based on the wave spectrum in Fig. 2, and then statistically processing this time series to obtain the joint distribution of the wave crest height and period. We can obviously find that the results from the linear simulation fit poorer to the real distribution than the results from the transformed linear simulation do. By comparing Figs. 4 and 5, the obvious improvement is that the results in the period range (4s-7s) and the height range 7m-8m where the new method is better than the traditional method. For some waves with very high crest heights (e. g. >7m), the traditional linear simulation method predicts too lower crest heights corresponding to a specific wave period.

In Fig. 6 the solid black lines again represent the results of the joint distribution of the wave crest height and period directly obtained from the measured wave elevation points at the Gulfaks C platform. In Fig. 6 the solid green lines represent the results of the joint distribution of the wave crest height and period obtained from using the nonlinear simulation method, i.e. by numerically implementing Eq. (14) to generate a time series of sea waves with 200000 elevation points, and then statistically processing this time series to obtain the joint distribution of the wave crest height and period. In this case, it takes about 247 s on a desktop computer (HP dx2310MT (VP784PA), Pentium (R) Dual-Core CPU E5300 @2.60GHz) to obtain the green curves in Fig. 6 by using the nonlinear simulation method. If we look more closely to Figs. 6 and 4 and compare them, we can find that the results from the nonlinear simulation still fit somewhat poorer to the real distribution than the results from the transformed linear simulation do. For some waves with very high crest heights (e. g. in the range of 7−8m), the nonlinear simulation method predicts too shorter

**Table 1**
The joint wave crest height and period probability densities obtained from the measured Gulfaks data.

| $A_c$ (m) | $T_c$ (s) | | | | | | | |
|---|---|---|---|---|---|---|---|---|
| | 5.04 | 5.12 | 5.19 | 5.26 | 5.34 | 5.41 | 5.49 | 5.56 |
| 7.60 | 0.0004060 | 0.0003898 | 0.0003769 | 0.0003687 | 0.0003621 | 0.000355 | 0.0003502 | 0.0003474 |
| 7.64 | 0.0003568 | 0.0003433 | 0.0003349 | 0.0003311 | 0.0003271 | 0.0003237 | 0.0003244 | 0.000325 |
| 7.69 | 0.0003141 | 0.0003032 | 0.0002973 | 0.0002961 | 0.0002953 | 0.0002964 | 0.0003011 | 0.000304 |

**Table 2**
The joint wave crest height and period probability densities obtained from the nonlinear simulation method.

| $A_c$ (m) | $T_c$ (s) | | | | | | |
|---|---|---|---|---|---|---|---|
| | 4.98 | 5.07 | 5.16 | 5.25 | 5.35 | 5.44 | 5.53 |
| 7.58 | 0.000100 | 0.000100 | 0.000100 | 0.000100 | 0.000100 | 0.000100 | 0.000100 |
| 7.62 | 0.000100 | 0.000100 | 0.000100 | 0.000100 | 0.000100 | 0.000100 | 0.000100 |
| 7.67 | 0.000100 | 0.000100 | 0.000100 | 0.000100 | 0.000100 | 0.000100 | 0.000100 |
| 7.72 | 0.000100 | 0.000100 | 0.000100 | 0.000100 | 0.000100 | 0.000100 | 0.000100 |

**Table 3**
The joint wave crest height and period probability densities obtained from the transformed linear simulation method.

| $A_c$ (m) | $T_c$ (s) | | | | | | |
|---|---|---|---|---|---|---|---|
| | 5.04 | 5.14 | 5.23 | 5.33 | 5.42 | 5.52 | 5.61 |
| 7.59 | 0.00020 | 0.00020 | 0.00020 | 0.00020 | 0.00020 | 0.00014 | 0.00013 |
| 7.65 | 0.00015 | 0.00015 | 0.00015 | 0.00014 | 0.00013 | 0.00011 | 0.00010 |
| 7.71 | 0.00013 | 0.00013 | 0.00012 | 0.00011 | 0.00010 | 0.00010 | 0.00010 |

corresponding periods. In case of some waves of very long ($T_c$) and small ($A_c$) the curves in Fig. 6 are also agreeing much poorer. The aforementioned research results demonstrate that our proposed transformed linear simulation method has higher accuracy and efficiency for predicting the joint distribution of the wave crest height and period than the nonlinear simulation method does.

It should be further noted that the transformed linear simulation method is not a certain approximation to the nonlinear simulation method. The transformed linear simulation method is not an extension of the nonlinear simulation method. These are two entirely different techniques. The nonlinear simulation method is obviously a numerical technique. However, strictly speaking, the transformed linear simulation is an analytical method whose detailed procedures are specified in Section 2 of this paper. The nonlinear simulations of the first order waves and the second order correction waves are based on Eqs (7-14) in this paper while the random phase angles are designated to be uniformly distributed in the range of $[0, 2\pi]$. These nonlinearly simulated "uniformly" random waves do not include all of the natural variability of the real sea waves. On the contrary, the transformed linear simulation method focuses more on analytically following the intrinsic non-Gaussian nature of the real sea waves. Based on Eqs. (15-30) in this paper, the transformed linear simulation method obtained the results of the joint distribution of the wave crest height and period as shown in Fig. 4 in this paper, and these results turn out to fit the measured wave data very well.

In order to give some quantitative comparisons besides using the above figures (Figs. 3–6), we have summarized some values of the joint wave crest height and period probability densities obtained using various methods in the following tables (Table 1-Table 3). Table 1 shows the values of the joint wave crest height and period probability densities for some waves with very high crest heights (in the range of 7.60–7.69m) and relatively short periods (in the range of 5.04–5.56s). These values are directly obtained from the measured wave elevation points at the Gulfaks C platform and are used as the benchmark for verifying the accuracy of the calculation results obtained using other methods. Table 2 summarizes the values of the joint wave crest height and period probability densities for some waves with very high crest heights (in the range of 7.58–7.72m) and relatively short periods (in the range of 4.98–5.53s) obtained using the nonlinear simulation method. Table 3 shows the values of the joint wave crest height and period probability densities for some waves with very high crest heights (in the range of 7.59–7.71m) and relatively short periods (in the range of 5.04–5.61s) obtained using the nonlinear simulation method. By carefully study the data in these three tables we can find that the joint probability density values obtained using the transformed linear simulation method are generally more close to the corresponding density values directly obtained from the measured wave elevation points at the Gulfaks C platform. For example the joint wave crest height ($Ac = 7.6m$) and period ($Tc = 5.04s$) probability density value 0.0002 obtained using the transformed linear simulation is more close to the corresponding benchmark value 0.000406, while the joint wave crest height ($Ac = 7.6m$) and period ($Tc = 5.04s$) probability density value 0.0001 obtained using the nonlinear simulation deviates more from the corresponding benchmark value 0.000406. These calculation results quantitatively demonstrate that our proposed transformed linear simulation method has higher accuracy for predicting the joint wave crest height and period probability densities than the nonlinear simulation method does.

Please note that from Fig. 5 we can already clearly notice that the joint wave crest height and period probability densities obtained using the linear simulation method deviate significantly from the corresponding benchmark values. Therefore, it is not necessary to add another table here containing the linear simulation results in order to save space for this article.

## 4. Conclusions

The detailed mathematical formulas of a proposed transformed linear simulation method for predicting the joint distributions of the wave heights and periods of nonlinear waves have been elucidated in this article, and the corresponding computer programs have also been developed. The basic points of the methodology proposed are as follows: The proposed transformed linear simulation method is based on a Hermite transformation model where the transformation is chosen to be a monotonic cubic polynomial, calibrated such that the first four moments of the transformed model match the moments of the true process. The

obtained Hermite transformation model is subsequently used to transform a linearly simulated wave elevation points time history into a non-Gaussian time series. Next, from this non-Gaussian time series the wave crest height and wave period time series are extracted. Then exact Epanechnikov kernel density estimates are carried out for obtaining the joint distribution of the wave crest height and period. The proposed new method has been utilized for calculating the joint distributions of the wave height and period of a sea state with the surface elevation data measured at the Gulfaks C platform in the North Sea, and its accuracy and efficiency have been demonstrated to be higher than those of the linear and nonlinear simulation methods. The research results in this paper demonstrate that our proposed transformed linear simulation method can be utilized by engineers as a valuable tool for predicting the joint distributions of the wave height and period in their ocean engineering design projects.

## Acknowledgment

## References

Cavanié, A., Arhan, M., Ezraty, R., 1976. A statistical relationship between individual heights and periods of storm waves. In: Proceedings of the Behavior of Offshore Structures (BOSS), pp. 354—363.

Hasselmann, K., 1962. On the non-linear energy transfer in a gravity-wave spectrum, Part 1, General Theory. J. Fluid Mech. 12, 481—500.

Langley, R.S., 1987. A statistical analysis of non-linear random waves. Ocean Eng. 14 (5), 389—407.

Lindgren, G., Rychlik, J., 1982. Wave characteristics distributions for Gaussian waves — wave length, amplitude and steepness. Ocean Eng. 9, 411—432.

Liu, D.Y., Ma, Y.X., Dong, G.H., Perlin, M., 2015. An experimental study of weakly three-dimensional non-breaking and breaking waves. Eur. J. Mech. B Fluid 52, 206—216.

Liu, D.Y., Ma, Y.X., Dong, G.H., Perlin, M., 2016. Detuning and wave breaking during nonlinear surface wave focusing. Ocean Eng. 113, 215—223.

Longuet-Higgins, M.S., 1975. On the joint distribution of the periods and amplitudes of sea waves. J. Geophys. Res. 80 (18), 2688—2694.

Longuet-Higgins, M.S., 1983. On the joint distribution of wave periods and amplitudes in a random wave field. Proc. R. Soc. A-Math. Phys. Eng. Sci. 389, 241—258.

Ma, Y.X., Dong, G.H., Liu, S.X., Zang, J., Li, J.X., Sun, Y.Y., 2010. Laboratory study of unidirectional focusing waves in intermediate depth water. J. Eng. Mech-ASCE 136 (1), 78—90.

Ochi, M.K., 2005. Ocean Waves, the Stochastic Approach. Cambridge University Press.

Perlin, M., Choi, W., Tian, Z., 2013. Breaking waves in deep and intermediate waters. Annu. Rev. Fluid Mech. 45, 115—145.

Rodríguez, G.R., Soares, C.G., 1999. The bivariate distribution of wave heights and periods in mixed sea states. J. Offshore Mech. Arct. Eng. Trans. ASME 121 (2), 102—108.

Rodríguez, G.R., Royo, F.R., Pacheco, M., Martínez, A., 1999. On the joint distribution of wave heights and periods: the role of the spectral bandwidth. J. Offshore Mech. Arct. Eng. Trans. ASME 121 (3), 187—193.

Stansell, P., Wolfram, J., Linfoot, B., 2004. Improved joint probability distribution for ocean wave heights and periods. J. Fluid Mech. 503, 273—297.

Toffoli, A., Onorato, M., Monbaliu, J., 2006. Wave statistics in unimodal and bimodal seas from a second-order model. Eur. J. Mech. B Fluid 25, 649—661.

Wang, Y.G., 2014. Calculating crest statistics of shallow water nonlinear waves based on standard spectra and measured data at the Poseidon platform. Ocean Eng. 87, 16—24.

Wang, Y.G., Xia, Y.Q., 2012. Simulating mixed sea state waves for marine design. Appl. Ocean Res. 37, 33—44.